Measurement Accuracy of Ultrasound Viscoelastic Creep Imaging in Measuring the Viscoelastic Properties of Heterogeneous Materials

Che-Yu Lin[*], Yi-Cheng Chen, Chin Pok Pang, Tung-Han Yang

Institute of Applied Mechanics, College of Engineering, National Taiwan University, Taipei, Taiwan

Abstract

Ultrasound viscoelastic creep imaging (UVCI) is a newly developed technology aiming to measure the viscoelastic properties of materials. The purpose of this study is to investigate the accuracy of UVCI in measuring the viscoelastic properties of heterogeneous materials that mimic pathological lesions and normal tissues. The finite element simulation is used to investigate the measurement accuracy of UVCI on three material models, including a homogeneous material, a single-inclusion phantom, and a three-layer structure. The measurement accuracy for a viscoelastic property is determined by the difference between the simulated measurement result of that viscoelastic property and its true value defined during the simulation process. The results show that UVCI in general cannot accurately measure the true values of the viscoelastic properties of a heterogeneous material, demonstrating the need to further improve the theories and technologies relevant to UVCI to improve its measurement accuracy on tissue-like heterogeneous materials.

1. Introduction

Ultrasound elastography, or called ultrasound elasticity imaging, is an advanced ultrasound-imaging-based technology that aims to noninvasively measure the mechanical properties of tissues [1-3]. The initial description of ultrasound elastography appeared in the early 1990s [4]. Subsequently, the development of its relevant technologies and the feasibility studies for investigating its application potential has become one of the most popular research topics [5]. Soon, ultrasound elastography has developed into a real-time clinical tool capable of diagnosing pathologies of tissues based on serving the parameters relevant to the stiffness of tissues as biomarkers [6-10]. This rationale for diagnosis is based on the fact that pathological processes may cause changes in the stiffness of tissues [9, 11-13].

Despite the fact that ultrasound elastography has been widely applied in research to measure the stiffness of various tissues such as breast, liver, and musculoskeletal tissues, its clinical usefulness has not been assured. It is because, in part, the stiffness alone (the single metric that ultrasound elastography measures) could not be sufficient to completely describe the mechanical condition of tissues [14-15]. The stiffness is just a single parameter that describes the combined effect of mechanical properties. However, biological tissues are all viscoelastic, meaning that tissues possess both fluid-like and solid-like properties [16-18]. Changes in the status of tissues due to pathologies lead to changes in both fluid-like and solid-like properties, resulting in changes in viscoelastic properties of tissues [15, 19-20]. In order to more completely evaluate the health status of tissues in terms of their mechanical properties, it is important to measure the viscoelastic properties rather than just the stiffness alone.

[*] Corresponding author. E-mail address: cheyu@ntu.edu.tw

Tel.: +886-2-33665653; Fax: +886-2-23639290
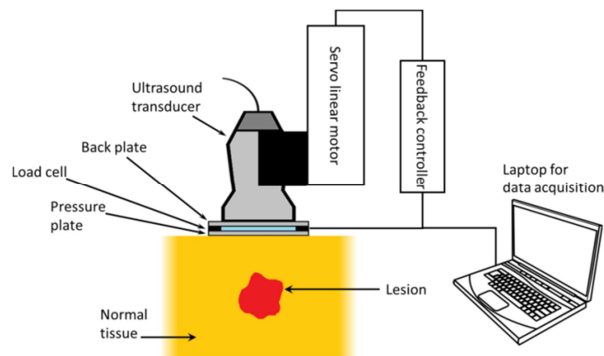
Fig. 1 Illustration of the ultrasound viscoelastic creep imaging system

In recent years, a research group [21-24] has proposed a novel ultrasound imaging technology called ultrasound viscoelastic creep imaging (UVCI) aiming to noninvasively measure the viscoelastic properties of tissues, as illustrated in Fig. 1. Compared to ultrasound elastography that can only measure the stiffness, UVCI can measure several parameters relevant to the viscoelastic properties of tissues, and therefore may have a greater potential to be a useful clinical tool to provide a more thorough evaluation of the mechanical condition and health statue of tissues. Compared to traditional mechanical testing methods such as uniaxial tensile and compressive testings, multiaxial testing, and shear rheometer testing that can only measure the bulk properties of materials, UVCI can quantitatively measure the internal spatial distribution of the viscoelastic properties of materials. In addition, compared to traditional mechanical testing systems, an ultrasound-imaging-based technology such as UVCI should be portable, lighter, and easier to apply for in vivo studies on human tissues.

In order to further understand how useful UVCI can be applied in the field of clinical diagnosis, this study intends to quantitatively investigate the accuracy of UVCI in measuring the viscoelastic properties of tissue-like heterogeneous materials. The main study question is: can UVCI accurately measure the true viscoelastic properties of each portion in a heterogeneous material? For this study purpose, finite element simulation is utilized in the present study, and it is believed that computer simulation is the most appropriate methodology that can fulfill this study purpose because the theoretical parameters defined during the simulation process can be served as the golden standard to be compared with the results obtained from the simulation for verifying the measurement accuracy of UVCI.

2. Literature Review

In literature, UVCI has been used to measure the viscoelastic properties of homogeneous and heterogeneous tissue-like phantoms, as well as benign and malignant human breast lesions in vivo [21-24]. These studies have consistently concluded that UVCI can provide accurate measurements of the viscoelastic properties of these samples. However, by observing some of the color images illustrated in these studies that display the spatial distribution of the viscoelastic properties (for example, Fig. 6 in [22], Figs. 2 and 3 in [24]), it can be observed that the contrast of the image is not high. It means that, the color of an area in the image suspected as where the lesion locates is similar to the color of many other areas; therefore, the lesion cannot be clearly identified in the image and cannot be specifically distinguished from many other areas in the image. Fig. 2 shows an example.

The problem mentioned above could be due to the imperfect function of UVCI, or due to the heterogeneous nature of in vivo tissues. However it may be, the lack of high contrast in the image may decrease the success rate of clearly identifying pathological lesions, and decrease the accuracy to measure the true viscoelastic properties of tissues. Consequently, the esteem of UVCI for clinical and biomedical applications could be hampered. Hence, even though some exciting preliminary results have been reported in literature [21-24], it is still unclear whether or not UVCI can be successfully applied to heterogeneous materials and structures such as pathological lesions and tumors in a tissue. This issue raises the motivation of the present study to investigate the accuracy of UVCI in measuring the viscoelastic properties of tissue-like heterogeneous materials, in order to understand the potential of UVCI as a tool to be applied in the field of clinical diagnosis.

(a) B-mode ultrasound image   (b) Spatial distribution map of mechanical properties
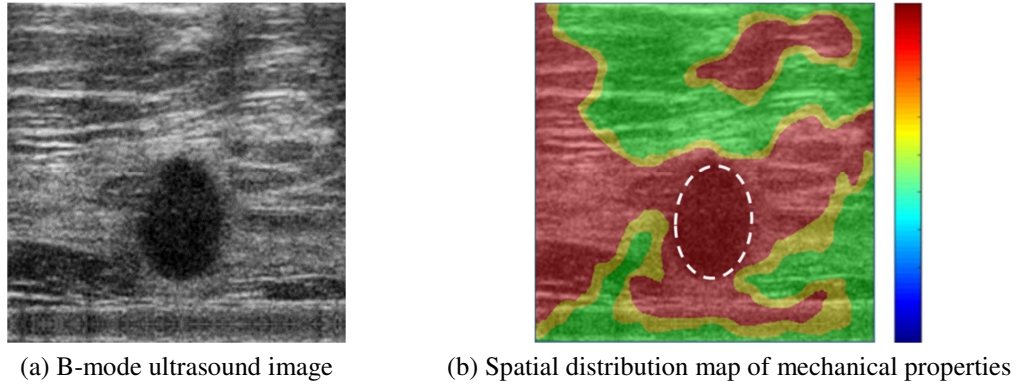
Fig. 2 An example showing a spatial distribution map of the viscoelastic properties with low contrast

3. Materials and Methods

3.1. Introduction to ultrasound viscoelastic creep imaging

The principle of UVCI is similar to that of mechanical creep testing, in which a constant load is applied to the sample for a period of time to induce the viscoelastic creep behavior. By recording the creep data using ultrasound imaging and then analyzing (i.e., curvefitting) the creep data using a viscoelastic mathematical model, the viscoelastic properties of the sample can be quantitatively evaluated. In UVCI, the ultrasound transducer is used to exert a uniform compression force on the sample's top surface. The automatic motion control of the transducer is achieved using a linear motor. The magnitude of compression force, measured using the load cells embedded between the two plates attached to the transducer, is instantly monitored and controlled by a feedback controller. The axial strain of each material point within the sample is measured using ultrasound imaging.

For the measurement, the transducer is continuously moved downward by a consistent loading rate to compress the sample, until the magnitude of compression force attains a prescribed maximal value. The load is applied using an extremely rapid loading rate (the duration from the beginning to maximal compression force is 1/6 s), such that the load can be approximated as a step load. Once the prescribed maximal compression force is attained, the compression force is thereupon kept constant for a time period. Since the compression force on the sample's top surface is constant, the axial stress of each material point within the sample should also be constant. Hence, according to the principle of viscoelasticity, during the time period when the stress of each material point within the sample is constant, all material points within the sample exhibit creep (Fig. 3). The strain-time relationship during creep (i.e., the creep curve) of each material point can be described by the following equation derived using the standard linear solid model Maxwell form (Fig. 3) based on the assumption that the load is a step load [18]:

$$\varepsilon(t) = \frac{\sigma_0}{E}(1 - g \cdot e^{\frac{-t}{\tau_C}}) \tag{1}$$

where $\varepsilon(t)$ is the axial strain as a function of time. E is the modulus of elasticity. g is a parameter relevant to the viscoelastic properties [18]. τ_C is equal to $\tau_R/(1 - g)$, where τ_C is the retardation time constant while τ_R is the relaxation time constant, and these two parameters are relevant to the viscoelastic properties. σ_0 is the axial stress at the beginning of creep (i.e., the axial stress at $t = 0$) as well as the constant axial stress during creep. In the present study, σ_0 is set as the magnitude of compression force on the sample's top surface.

The viscoelastic properties of each material point are quantitatively evaluated through curvefitting the creep curve of each material point by Eq. (1). The viscoelastic properties of all material points are then used to construct the 2D spatial distribution maps of the viscoelastic properties of the entire sample.
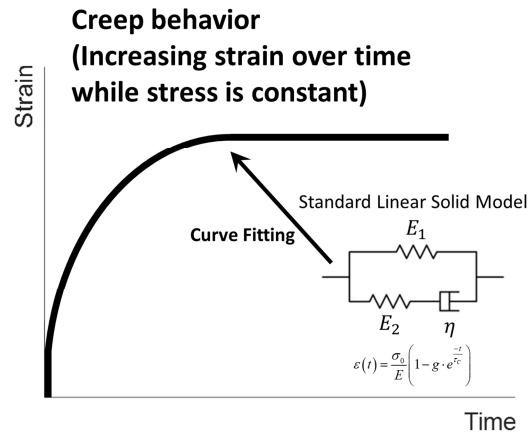
Fig. 3 Evaluation of the viscoelastic properties using the standard linear solid model to curvefit the creep curve

3.2. *Finite element simulation and data analysis*

In the present study, the accuracy of UVCI in measuring the viscoelastic properties of heterogeneous materials is studied by finite element simulation. The package ABAQUS/CAE 2021 (Dassault Systems Simulia Corp., Johnson, RI, USA) is used to perform the finite element simulation. The finite element models used in the present study are all 3D axisymmetric cylindrical models. There are three material models investigated in the present study, and their dimensions are described as follows:

(1) Homogeneous material (Fig. 4): The thickness and radius of the model are 50 and 25 mm, respectively. The model meshes with quadrilateral elements of dimensions 0.5×0.5 mm. The element number and the node number in the model are 5000 and 5284 nodes respectively.

(2) Single-inclusion phantom (Fig. 4): The thickness of the entire model is 50 mm while its radius is 25 mm. The thickness of the inclusion is 15 mm while its radius is 7.5 mm. The model meshes with quadrilateral elements of dimensions 0.5×0.5 mm. The element number and the node number in the model are 5000 and 5284 nodes respectively.

(3) Three-layer structure (Fig. 4): The thickness of the entire model is 30 mm while its radius is 25 mm. The model has three layers with consistent dimensions. The thickness of each layer is 10 mm while its radius is 25 mm. The model meshes with quadrilateral elements of dimensions 0.5×0.5 mm. The element number and the node number in the model are 3000 and 3213 nodes respectively.

(a) Homogeneous material   (b) Single-inclusion phantom   (c) Three-layer structure
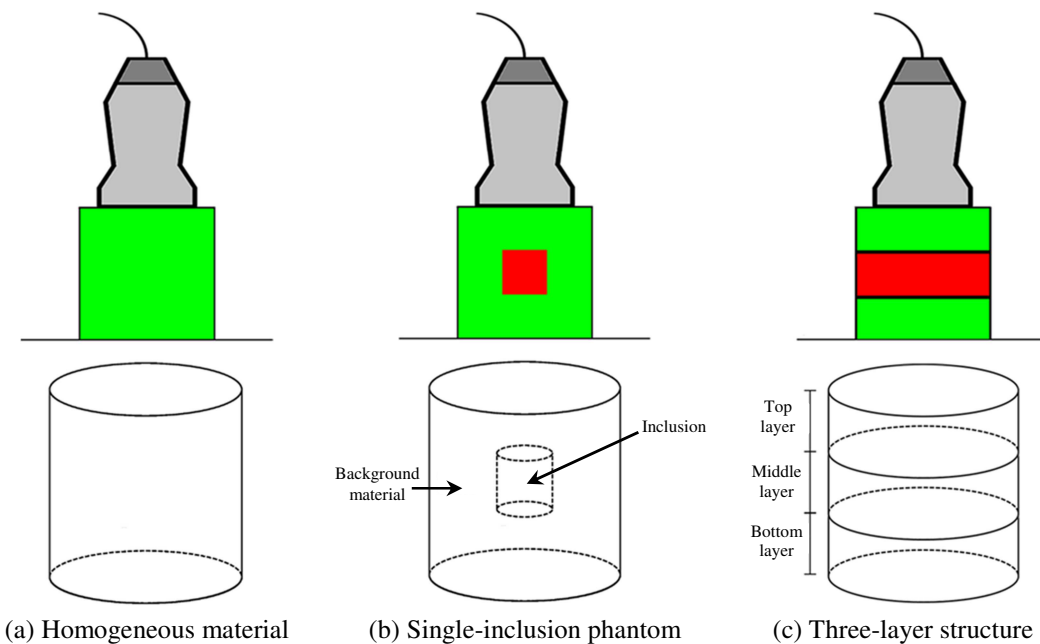
Fig. 4 Illustration of three material models investigated in the present study

The settings of the boundary conditions and mechanical properties for all three material models are the same, described as follows. The boundary conditions are that, the model's bottom is constrained along the axial direction, and its top and sides are not constrained. The material that constructs the model is assumed to be linearly viscoelastic, isotropic, and incompressible. The mechanical properties of the material are defined by four parameters: the modulus of elasticity (E), the Poisson's ratio, τ_R and g. τ_R and g are two parameters relevant to the viscoelastic properties, defined using the one-branch Prony series of the dimensionless relaxation modulus.

$$g_R(t) = 1 - g(1 - e^{\frac{-t}{\tau_R}})$$

(2)

where τ_R and g are the same parameters in Eq. (1); that is, τ_R is the relaxation time constant while g is a parameter relevant to the viscoelastic properties [18]. g is set as a constant of 0.8 in the present study. Since the material is assumed to be incompressible, the Poisson's ratio is set as 0.495 (the maximal Poisson's ratio that can be set in ABAQUS).

In the simulation, a uniform and constant compression pressure (1000 Pa) is applied on the model's top surface. The load is applied using an extremely rapid loading rate (the duration from the beginning to maximal compression force is 1/6 s). Once the prescribed maximal compression pressure is attained, the compression pressure is thereupon kept constant for a time period (set as 1000 s in the present study), during which the creep behavior occurrs. That is, the strain of each element of the model increases with time until a constant strain is attained. The strain-time data (i.e., the creep curve) of each element is recorded for further analysis. Then, a MATLAB-based B-mode ultrasound imaging simulation tool [25-27] is used to convert each element's raw strain-time data to the simulated strain-time data obtained from B-mode ultrasound imaging system with the characteristics of pulse-echo ultrasound signals. Fig. 5 is an example that shows the comparison between an original spatial distribution map of a viscoelastic property of the homogeneous material (Fig. 5(a)) and the corresponding map with simulated pulse-echo ultrasound signals of B-mode ultrasound imaging (Fig. 5(b)). The randomly scattered dots that can be observed in Fig. 5(b) reflect the simulated pulse-echo ultrasound signals of B-mode ultrasound imaging.

The creep curve of each element is curvefitted using Eq. (1) for obtaining the two parameters relevant to the viscoelastic properties (E and τ_R) of each element. Please note that, according to Eq. (1), there are actually three viscoelastic parameters, i.e., E, τ_R, and g, but only E and τ_R are considered in the data analysis since g is set as a constant in the simulation. The curve fitting is performed using MATLAB (R2022a; Mathworks, Natick MA) [30]. The values of E and τ_R of each element yielded by the curve fitting are regarded as the viscoelastic properties of each element measured by UVCI obtained from the simulation. Once the viscoelastic properties of all elements are obtained, the 2D spatial distribution map for each viscoelastic property (E and τ_R) of the material model can be developed. However, because of the axisymmetric nature of the finite element model, the currently-obtained map is just half of that obtained from UVCI in reality. Hence, the current map is combined with its reflection to obtain the full map that should be obtained in a real UVCI measurement.

(a) Original map   (b) Map with simulated ultrasound signals
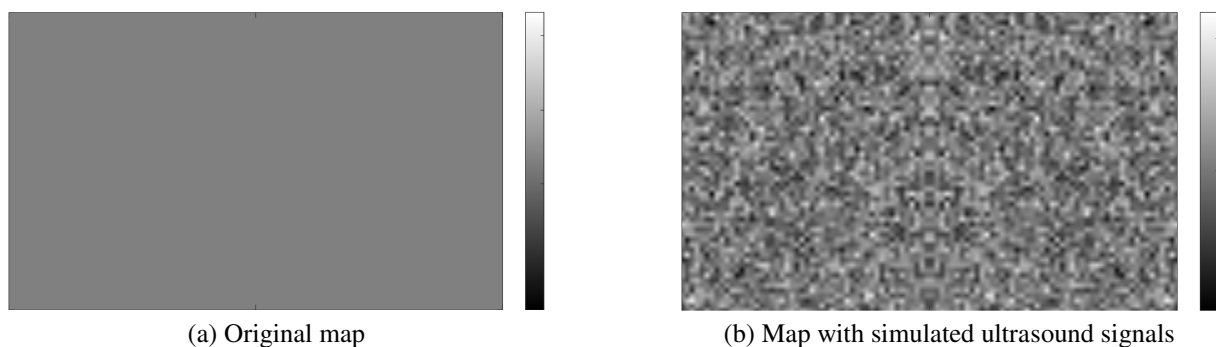
Fig. 5 Comparison between the original map and the corresponding map with simulated ultrasound signals

The settings of the theoretical viscoelastic properties during the simulation in ABAQUS for each material model are described as follows:

(1) Homogeneous material: E is set as 10000 Pa, while τ_R is set as 1 s.

(2) Single-inclusion phantom: E of the background material is fixed as 10000 Pa, while τ_R of the background material is fixed as 1 s. E of the inclusion is 1000, 5000, 10000, and 20000 Pa respectively, while τ_R of the inclusion is 0.5, 1, and 2 s respectively. Hence, eleven simulation tests in total will be conducted, excluding the case in which the material is homogeneous with E and τ_R of the inclusion are 10000 Pa and 1 s respectively.

(3) Three-layer structure: E of the top and bottom layers is fixed as 10000 Pa, while τ_R of the top and bottom layers is fixed as 1 s. E of the middle layer is 1000, 5000, 10000, and 20000 Pa respectively, while τ_R of the middle layer is 0.5, 1, and 2 s respectively. Hence, eleven simulation tests in total will be conducted, excluding the case in which the material is homogeneous with E and τ_R of the middle layer are 10000 Pa and 1 s respectively.

The measurement accuracy of UVCI for a viscoelastic property (E or τ_R) is determined by the difference between the simulation value (i.e., the value of that viscoelastic property obtained from the simulation) and the theoretical value (i.e., the value of that viscoelastic property defined in ABAQUS). The smaller the difference between them, the higher the measurement accuracy. This difference is quantified using the following equation:

$$\text{error}\,(\%) = \frac{\left|\text{simulation value} - \text{theoretical value}\right|}{\text{theoretical value}} \tag{3}$$

If the error is smaller than 5%, the simulation and theoretical values are close enough to each other and the measurement is regarded as accurate. The simulation value of a viscoelastic property of a portion (i.e., the background material and inclusion of the single-inclusion phantom, and the top, middle, and bottom layers of the three-layer structure) in the model is defined as the average value of that property of all elements in that portion obtained from the simulation.

4. Results

Fig. 6 shows a set of examples of the spatial distribution maps of the viscoelastic properties (E and τ_R) for each material model. Some observations from Fig. 6 can be highlighted:

(1) Homogeneous material: The maps of both properties are homogeneous, as expected.

(2) Heterogeneous materials, including the single-inclusion phantom and the three-layer structure: The map of a property (i.e., (E or τ_R) of a portion (i.e., the background material and inclusion of the single-inclusion phantom, as well as the top, middle, and bottom layers of the three-layer structure) is not homogeneous, although in theory it should be homogeneous (since the theoretical value of a property of a portion is set as a single value during the simulation). In addition, there are larger errors and stronger inhomogeneities near the boundaries of a portion.
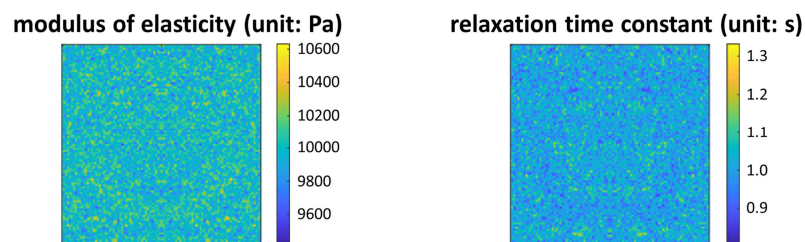
(a) Homogeneous material

Fig. 6 Examples of the spatial distribution maps of the viscoelastic properties for each material model

modulus of elasticity (unit: Pa)　　　relaxation time constant (unit: s)

(b) Single-inclusion phantom

modulus of elasticity (unit: Pa)　　　relaxation time constant (unit: s)

(c) Three-layer structure
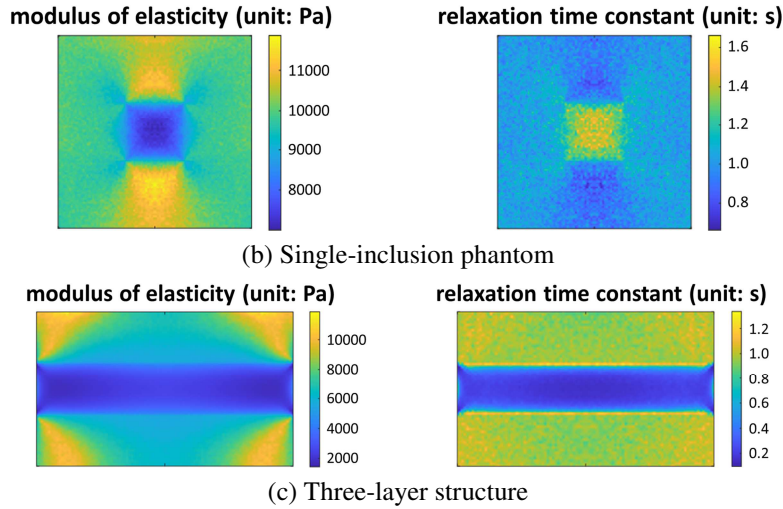
Fig. 6 Examples of the spatial distribution maps of the viscoelastic properties for each material model (continued)

Table 1 Simulation results for the homogeneous material

Theoretical properties of the homogeneous material		Simulation properties of the homogeneous material		Error (%)	
E (Pa)	τ_R (s)	E (Pa)	τ_R (s)	E	τ_R
10000	1	10000	1.016	0.00 *	0.02 *

Note: The error value of the case, in which the error is lower than 5% and the measurement is accurate, is marked with an asterisk and underline.

Table 2 Simulation results for the background material of the single-inclusion phantom

Theoretical properties of the inclusion		Simulation properties of the background material		Error (%)	
E (Pa)	τ_R (s)	E (Pa)	τ_R (s)	E	τ_R
1000	0.5	10231	1.009	2.31 *	0.94 *
1000	1	10233	1.008	2.33 *	0.83 *
1000	2	10226	1.004	2.26 *	0.36 *
5000	0.5	10042	1.016	0.42 *	1.60 *
5000	1	10046	1.013	0.46 *	1.31 *
5000	2	10038	1.012	0.38 *	1.18 *
10000	0.5	9996	1.015	0.04 *	1.51 *
10000	2	9999	1.017	0.01 *	1.67 *
20000	0.5	10021	1.014	0.21 *	1.41 *
20000	1	10025	1.017	0.25 *	1.74 *
20000	2	10025	1.026	0.25 *	2.59 *

Note: The error value of the case, in which the error is lower than 5% and the measurement is accurate, is marked with an asterisk and underline.

Table 3 Simulation results for the inclusion of the single-inclusion phantom

Theoretical properties of the inclusion		Simulation properties of the inclusion		Error (%)	
E (Pa)	τ_R (s)	E (Pa)	τ_R (s)	E	τ_R
1000	0.5	6206	1.036	520.58	107.27
1000	1	6199	1.071	519.86	7.15
1000	2	6211	1.146	521.14	42.69
5000	0.5	7948	0.911	58.95	82.11
5000	1	7953	1.026	59.05	2.56 *
5000	2	7948	1.319	58.95	34.05
10000	0.5	10012	0.825	0.12 *	64.99
10000	2	10030	1.457	0.30 *	27.17
20000	0.5	14108	0.735	29.46	46.95
20000	1	14098	1.003	29.51	0.33 *
20000	2	14128	1.611	29.36	19.43

Note: The error value of the case, in which the error is lower than 5% and the measurement is accurate, is marked with an asterisk and underline.

Table 4 Simulation results for the top layer of the three-layer structure

Theoretical properties of the middle layer		Simulation properties of the top layer		Error (%)	
E (Pa)	τ_R (s)	E (Pa)	τ_R (s)	E	τ_R
1000	0.5	7494	0.951	25.06	4.88 *
1000	1	7481	0.979	25.19	2.15 *
1000	2	7489	1.056	25.11	5.60
5000	0.5	8823	0.928	11.77	7.22
5000	1	8813	1.003	11.87	0.27 *
5000	2	8830	1.180	11.70	17.96
10000	0.5	10018	0.915	0.18 *	8.54
10000	2	10026	1.228	0.26 *	22.76
20000	0.5	11739	0.914	17.39	8.59
20000	1	11706	1.029	17.06	2.85 *
20000	2	11758	1.265	17.58	26.48

Note: The error value of the case, in which the error is lower than 5% and the measurement is accurate, is marked with an asterisk and underline.

Table 5 Simulation results for the middle layer of the three-layer structure

Theoretical properties of the middle layer		Simulation properties of the middle layer		Error (%)	
E (Pa)	τ_R (s)	E (Pa)	τ_R (s)	E	τ_R
1000	0.5	2712	0.826	171.24	65.10
1000	1	2692	1.232	169.25	23.17
1000	2	2703	2.004	170.30	0.21 *
5000	0.5	6760	0.776	35.20	55.22
5000	1	6726	1.058	34.53	5.81
5000	2	6746	1.629	34.92	18.57
10000	0.5	10021	0.722	0.21 *	44.49
10000	2	10025	1.651	0.25 *	17.46
20000	0.5	15860	0.649	20.7	29.86
20000	1	15834	0.989	20.83	1.06 *
20000	2	15861	1.713	20.69	14.33

Note: The error value of the case, in which the error is lower than 5% and the measurement is accurate, is marked with an asterisk and underline.

Table 6 Simulation results for the bottom layer of the three-layer structure

Theoretical properties of the middle layer		Simulation properties of the bottom layer		Error (%)	
E (Pa)	τ_R (s)	E (Pa)	τ_R (s)	E	τ_R
1000	0.5	7342	0.957	26.58	4.27 *
1000	1	7349	0.979	26.51	2.12 *
1000	2	7345	1.054	26.55	5.41
5000	0.5	8690	0.920	13.10	7.99
5000	1	8682	1.000	13.18	0.03 *
5000	2	8700	1.190	13.00	19.00
10000	0.5	10024	0.897	0.24 *	10.28
10000	2	10033	1.262	0.33 *	26.20
20000	0.5	11964	0.904	19.64	9.60
20000	1	11943	1.036	19.43	3.63 *
20000	2	11991	1.301	19.91	30.13

Note: The error value of the case, in which the error is lower than 5% and the measurement is accurate, is marked with an asterisk and underline.

Table 1 shows the simulation results for the homogeneous material, showing the comparison between the simulation and theoretical properties. Tables 2 and 3 show the simulation results for the background material and inclusion of the single-inclusion phantom respectively, showing how the simulation properties of the background material and inclusion change with the theoretical properties of the inclusion. Tables 4, 5, and 6 show the simulation results for the top, middle, and bottom layers of the three-layer structure respectively, showing how the simulation properties of the top, middle, and bottom

layers change with the theoretical properties of the middle layer. The simulation results shown in these tables demonstrate the measurement accuracy of UVCI. Some observations from Tables 1 to 6 can be highlighted:

(1) Homogeneous material: The simulation property is almost equal to the theoretical property, showing that UVCI can accurately measure the viscoelastic properties of the homogeneous material.

(2) Single-inclusion phantom: The measurement of E or τ_R of the background material is accurate in each case. However, for the inclusion, the measurements of both properties are inaccurate in most cases, showing that UVCI in general cannot accurately measure the viscoelastic properties of the inclusion of the single-inclusion phantom. The measurement of a property of the inclusion can be accurate if and only if when the background material and inclusion have the same value of that property.

(3) Three-layer structure: For all three layers, the measurements of both properties are inaccurate in most cases, showing that UVCI in general cannot accurately measure the viscoelastic properties of the three respective layers of the three-layer structure. The measurement of a property of a layer can be accurate if and only if when all three layers have the same value of that property.

5. Discussion

The idea of developing UVCI technology is to provide a clinical diagnostic tool for quantifying the severity of pathologies based on serving the viscoelastic properties of tissues as biomarkers. This idea is based on the fact that pathological processes could result in changes of the viscoelastic properties of tissues, and therefore there could be a correlation between the viscoelastic properties of tissues and the severity of pathologies. However, the findings of the present study demonstrate that UVCI cannot accurately measure the viscoelastic properties of the inclusion of the single-inclusion phantom and those of the three respective layers of the three-layer structure, although it can accurately measure the viscoelastic properties of the homogeneous material and those of the background material of the single-inclusion phantom. These findings suggest that UVCI in general cannot accurately measure the true values of the viscoelastic properties of a single material point as well as a portion of a heterogeneous material.

The clinical implication of the findings of the present study is that, it could be difficult to apply UVCI as a clinical tool to accurately and quantitatively diagnose the severity of pathologies or the health status of tissues based on serving the true values of the viscoelastic properties of tissues as biomarkers. Fortunately, at least, UVCI can accurately measure the viscoelastic properties of homogeneous materials; therefore, it still has the potential to be a useful clinical tool to quantify the severity of pathologies and the health status of tissues that can be reasonably regarded as homogeneous, such as liver tissues.

The innovation of the present study is that, it is the first study to quantitatively and thoroughly investigate the accuracy of UVCI in measuring the viscoelastic properties of various kinds of heterogeneous materials by using finite element simulation, and the findings can help explain the experimental results in previous studies. Computer simulation is the necessary methodology for this study purpose. It is because, the theoretical parameters defined during the simulation process can be served as the golden standard to be compared with the simulation results for verifying the measurement accuracy of UVCI. It is one of the invaluable benefits of computer simulation. On the other hand, although direct experimental measurements on in vivo tissues can provide real measurement data, they actually cannot verify the measurement accuracy of UVCI since the viscoelastic properties of in vivo tissues are unknown (and to be determined) and therefore there is no golden standard to verify the experimental results.

By visually inspecting the spatial distribution maps of the viscoelastic properties obtained from UVCI (i.e., Fig. 6), different portions with different viscoelastic properties of a heterogeneous material could be clearly distinguished. For example, by visually inspecting Fig. 6, the inclusion can be distinguished from the background material of the single-inclusion

phantom, while the middle layer can be distinguished from the top and bottom layers of the three-layer structure. Hence, although UVCI cannot measure the true values of the viscoelastic properties of a portion of a heterogeneous material, it still could measure the relative values and could be useful to tell different portions of a heterogeneous material apart. Based on this feature, UVCI still could be a useful clinical tool for diagnosing the all-or-none presence or absence of pathology, although it could not be used to accurately quantify the severity of pathology.

In the future, in order to maximize UVCI's clinical and biomedical application values, there is an essential need to improve the measurement accuracy of UVCI on heterogeneous materials and structures by further improving the theories and technologies relevant to UVCI. It is because, after all, most biological tissues and biomaterials that UVCI aims to measure in real applications are heterogeneous. Three directions for improving the performance of UVCI are proposed as follows:

(1) In current UVCI technology, only the axial strain component of the sample is measured by ultrasound imaging. In addition, the constitutive equation applied to curvefit the creep curve for quantifying the associated viscoelastic properties, i.e. Eq. (1), is a one-dimensional mathematical model only considering axial strain and stress components. However, during the measurement using UVCI, the sample should undergo not only axial but also lateral stress and strain components under the compression of the ultrasound transducer, meaning that the mechanical behaviors (i.e., the states of stress and strain) of the sample should be two-dimensional in this situation. Hence, a one-dimensional constitutive equation could not be sufficient to completely describe and analyze the mechanical behehavior of the sample for accurately quantifying its viscoelastic properties. In the future, it is promising that the measurement accuracy of UVCI on heterogeneous materials and structures could be significantly improved, if both axial and lateral strain components can be measured by ultrasound imaging and a two-dimensional constitutive equation can be applied to analyze the measured data.

(2) In the future, a more detailed simulation analysis can be conducted to collect a large amount of data, and then a deep machine learning approach can be applied to construct a model that describes the relationship between the measured and theoretical (i.e., true) viscoelastic properties for each specific type of material. By serving the measured viscoelastic properties as the input of the established deep machine learning model, this model can be applied to reconstruct the true viscoelastic properties of the sample for obtaining accurate measurement results.

(3) Two published studies have proposed correction methods for improving the measurement accuracy of quantitative ultrasound imaging technologies [28-29]. It is suggested that these correction methods could be modified for use in improving the measurement accuracy of UVCI.

Although the structures of the heterogeneous material models (single-inclusion phantom and three-layer structure) used in the present simulation study are relatively simple compared to those of real tissues, they can appropriately mimic the main structural characteristics of some types of tissues. The structure of the single-inclusion phantom is similar to the nature of soft tissue tumors; therefore, the single-inclusion phantom is often chosen to model soft tissue tumors in both experimental and computational studies in literature. On the other hand, the three-layer structure is a natural configuration that can be often seen in some biological tissues and various kinds of biomaterials. In addition to their tissue-mimicking nature, single-inclusion phantom and three-layer structure are favorable for modeling tissues in research because they are easy to model and analyze due to their relatively simple geometries. Hence, it is believed that the single-inclusion phantom and three-layer structure are appropriate models for investigating the mechanical behaviors of normal and pathological tissues. Nevertheless, in the future, more realistic models are still needed to account for the complexity of real tissues in order to more accurately understand the actual mechanical behaviors of real tissues.

The UVCI technology investigated in the present study is also named compressional viscoelastography, a type of UVCI systems using mechanical compression (via the ultrasound transducer) as the source of the force excitation for inducing the stress field and creep behavior within the sample. In literature, several types of UVCI systems have been reported by different

research groups. These different UVCI systems are similar in fundamental principles, but there are still some key differences between them:

(1) The means of these UVCI systems to exert the force excitation are different and can be classified into two types, i.e., mechanical compression or acoustic radiation force.

(2) The acoustic-radiation-force based UVCI can only take the measurement at the focus of the acoustic radiation force, since only the magnitude of the acoustic radiation force at the focus is strong enough to induce significant deformation to be detected by ultrasound imaging. In other words, the acoustic-radiation-force based UVCI can only take the measurement at one single point at a time. On the other hand, the magnitude of the stress field induced by the mechanical-compression based UVCI is strong and uniformly distributed within the sample; therefore, the mechanical-compression based UVCI can take the measurement at each material point of a full cross-section of the sample and produce the 2D spatial distribution maps of viscoelastic properties.

(3) The magnitude of the acoustic radiation force at the focus is unknown in vivo, and therefore the acoustic-radiation-force based UVCI cannot obtain the true viscoelastic properties of in vivo tissues. It is because, two parameters, the absorption coefficient and the compressional sound speed of the sample, are needed to calculate the magnitude of the acoustic radiation force, but these two parameters are generally unknown for in vivo tissues. Similarly, for the mechanical-compression based UVCI, although the magnitude of the induced stress field is unknown in vivo, it is close to the known magnitude of the compressional pressure applied on the sample's top surface and could potentially be approximated using the principles of mechanics. Therefore, although the current mechanical-compression based UVCI cannot obtain the true viscoelastic properties of in vivo tissues either, it is believed that it could have a high potential for achieving that ultimate goal.

The present study has several limitations that should be carefully considered in future research:

(1) The material that constructs the computational models is assumed to be linearly viscoelastic, isotropic, and incompressible. In addition, the Poisson's ratio of the material is assumed to be a constant. However, a real tissue could be nonlinearly viscoelastic, anisotropic, and compressible, and its Poisson's ratio could be strain- and time-dependent. Therefore, due to these assumptions, the simulation results in the present study are just relative trends and should not be regarded as absolute relationships. However, this limitation does not violate the purpose of the present study that aims to provide relative trends for application guidelines.

(2) The dimensions of the models are not designed according to physical measures or a systematic methodology. In the future, it is essential to design the dimensions of the models according to those of real biological tissues and biomaterials, such that the simulation results could be more realistic. It is suggested that realistic tumor or tissue models can be constructed by real ultrasound images, such that the simulation and experimental results could be compared to each other.

(3) In this finite element simulation study, the settings of the factors that may affect the measurement accuracy (such as the loading and boundary conditions, dimensions and mechanical properties of materials, and so on) are specific. Therefore, the simulation results cannot be generalized to any situation. In the future, it is essential to explore the effects of different settings of these factors on the simulation results and conclusions.

6. Conclusions

In conclusion, the findings of the present finite element simulation study demonstrate that UVCI cannot accurately measure the viscoelastic properties of the inclusion of the single-inclusion phantom and those of the three respective layers of the three-layer structure. These findings suggest that UVCI in general cannot accurately measure the true values of the

viscoelastic properties of heterogeneous materials. The clinical implication of these findings is that, it could be difficult to apply UVCI as a clinical tool to accurately diagnose the severity of pathologies or the health status of tissues based on serving the viscoelastic properties of tissues as biomarkers, since most tissues are heterogeneous. However, at least, UVCI can accurately measure the viscoelastic properties of homogeneous materials. Therefore, it still has the potential to be a useful clinical tool to quantify the severity of pathologies and the health status of tissues that can be reasonably regarded as homogeneous, such as liver tissues. In addition, although UVCI cannot measure the true values of the viscoelastic properties of heterogeneous materials, it still could measure the relative values and could be useful to tell different portions of a heterogeneous material apart by visually inspecting the spatial distribution maps of the viscoelastic properties. Based on this feature, UVCI still could be a useful clinical tool for diagnosing the all-or-none presence or absence of pathology.

Conflicts of Interest

The authors declare no conflicts of interest.

Acknowledgments

References

[1] J. Bamber, et al., "EFSUMB Guidelines and Recommendations on the Clinical Use of Ultrasound Elastography. Part 1: Basic Principles and Technology," Ultraschall in der Medizin-European Journal of Ultrasound, vol. 34, no. 2, pp. 169-184, April 2013.

[2] T. Shiina, et al., "WFUMB Guidelines and Recommendations for Clinical Use of Ultrasound Elastography. Part 1: Basic Principles and Terminology," Ultrasound in Medicine and Biology, vol. 41, no. 5, pp. 1126-1147, May 2015.

[3] R. M. Sigrist, et al., "Ultrasound Elastography: Review of Techniques and Clinical Applications," Theranostics, vol. 7, no. 5, pp. 1303-1329, March 2017.

[4] J. Ophir, et al., "Elastography: A Quantitative Method for Imaging the Elasticity of Biological Tissues," Ultrasonic Imaging, vol. 13, no. 2, pp. 111-134, April 1991.

[5] A. Diker, et al., "A Novel Application Based on Spectrogram and Convolutional Neural Network for ECG Classification," 1st International Informatics and Software Engineering Conference, pp. 1-6, November 2019.

[6] J. Bercoff, et al., "Supersonic Shear Imaging: A New Technique for Soft Tissue Elasticity Mapping," IEEE Transactions on Ultrasonics, Ferroelectrics, and Frequency Control, vol. 51, no. 4, pp. 396-409, August 2004.

[7] L. Castera, et al., "Non-Invasive Evaluation of Liver Fibrosis Using Transient Elastography," Journal of Hepatology, vol. 48, no. 5, pp. 835-847, May 2008.

[8] M. Friedrich-Rust, et al., "Performance of Transient Elastography for the Staging of Liver Fibrosis: A Meta-Analysis," Gastroenterology, vol. 134, no. 4, pp. 960-974, April 2008.

[9] M. L. Palmeri, et al., "Acoustic Radiation Force-Based Elasticity Imaging Methods," Interface Focus, vol. 1, no. 4, pp. 553-564, June 2011.

[10] P. N. Wells, et al., "Medical Ultrasound: Imaging of Soft Tissue Strain and Elasticity," Journal of the Royal Society Interface, vol. 8, no. 64, pp. 1521-1549, June 2011.

[11] R. Masuzaki, et al., "Assessing Liver Tumor Stiffness by Transient Elastography," Hepatology International, vol. 1, no. 3, pp. 394-397, July 2007.

[12] J. R. Doherty, et al., "Acoustic Radiation Force Elasticity Imaging in Diagnostic Ultrasound," IEEE Transactions on Ultrasonics, Ferroelectrics, and Frequency Control, vol. 60, no. 4, pp. 685-701, March 2013.

[13] J. E. Brandenburg, et al., "Ultrasound Elastography: The New Frontier in Direct Measurement of Muscle Stiffness," Archives of Physical Medicine and Rehabilitation, vol. 95, no. 11, pp. 2207-2219, November 2014.

[14] C. Y. Lin, et al., "Effects of Loading and Boundary Conditions on the Performance of Ultrasound Compressional Viscoelastography: A Computational Simulation Study to Guide Experimental Design," Materials, vol. 14, no. 10, Article no. 2590, May 2021.

[15] C. Y. Lin, et al., "Investigating the Accuracy of Ultrasound Viscoelastic Creep Imaging for Measuring the Viscoelastic Properties of a Single-Inclusion Phantom," International Journal of Mechanical Sciences, vol. 199, Article no. 106409, June 2021.

[16] C. X. Deng, et al., "Ultrasound Imaging Techniques for Spatiotemporal Characterization of Composition, Microstructure, and Mechanical Properties in Tissue Engineering," Tissue Engineering Part B: Reviews, vol. 22, no. 4, pp. 311-321, February 2016.

[17] D. Huang, et al., "Viscoelasticity in Natural Tissues and Engineered Scaffolds for Tissue Reconstruction," Acta Biomaterialia, vol. 97, no. 1, pp. 74-92, October 2019.

[18] C. Y. Lin, "Alternative Form of Standard Linear Solid Model for Characterizing Stress Relaxation and Creep: Including a Novel Parameter for Quantifying the Ratio of Fluids to Solids of a Viscoelastic Solid," Frontiers in Materials, vol. 7, no. 11, Article no. 11, February 2020.

[19] C. Y. Lin, et al., "Quantitative Evaluation of the Viscoelastic Properties of the Ankle Joint Complex in Patients Suffering from Ankle Sprain by the Anterior Drawer Test," Knee Surgery, Sports Traumatology, Arthroscopy, vol. 21, no. 6, pp. 1396-1403, March 2013.

[20] I. Sack, et al., "Structure-Sensitive Elastography: On the Viscoelastic Powerlaw Behavior of in Vivo Human Tissue in Health and Disease," Soft Matter, vol. 9, no. 24, pp. 5672-5680, May 2013.

[21] A. Nabavizadeh, et al., "Automated Compression Device for Viscoelasticity Imaging," IEEE Transactions on Biomedical Engineering, vol. 64, no. 7, pp. 1535-1546, September 2016.

[22] M. Bayat, et al., "Automated in Vivo Sub-Hertz Analysis of Viscoelasticity (SAVE) for Evaluation of Breast Lesions," IEEE Transactions on Biomedical Engineering, vol. 65, no. 10, pp. 2237-2247, December 2017.

[23] A. Nabavizadeh, et al., "Viscoelastic Biomarker for Differentiation of Benign and Malignant Breast Lesion in Ultra-Low Frequency Range," Scientific Reports, vol. 9, no. 1, pp. 1-12, April 2019.

[24] M. Bayat, et al., "Multi-Parameter Sub-Hertz Analysis of Viscoelasticity with a Quality Metric for Differentiation of Breast Masses," Ultrasound in Medicine and Biology, vol. 46, no. 12, pp. 3393-3403, December 2020.

[25] D. Sheet, "Pseudo B-Mode Ultrasound Image Simulator," https://www.mathworks.com/matlabcentral/fileexchange/34199-pseudo-b-mode-ultrasound-image-simulator, February 24, 2022.

[26] J. C. Bamber, et al., "Ultrasonic B-Scanning: A Computer Simulation," Physics in Medicine and Biology, vol. 25, no. 3, Article no. 463, May 1980.

[27] Y. Yu, et al., "Speckle Reducing Anisotropic Diffusion," IEEE Transactions on Image Processing, vol. 11, no. 11, pp. 1260-1270, December 2002.

[28] M. R. Selzo, et al., "On the Quantitative Potential of Viscoelastic Response (VisR) Ultrasound Using the One-Dimensional Mass-Spring-Damper Model," IEEE Transactions on Ultrasonics, Ferroelectrics, and Frequency Control, vol. 63, no. 9, pp. 1276-1287, March 2016.

[29] M. M. Hossain, et al., "Electronic Point Spread Function Rotation Using a Three-Row Transducer for ARFI-Based Elastic Anisotropy Assessment: in Silico and Experimental Demonstration," IEEE Transactions on Ultrasonics, Ferroelectrics, and Frequency Control, vol. 68, no. 3, pp. 632-646, August 2020.

[30] M. Toğaçar, et al., "Tumor Type Detection in Brain MR Images of the Deep Model Developed Using Hypercolumn Technique, Attention Modules, and Residual Blocks," Medical and Biological Engineering and Computing, vol. 59, no. 1, pp. 57-70, November 2021.